A Lyapunov-based approach for Time-Coordinated 3D Path-Following of Multiple Quadrotors

Venanzio Cichella, Isaac Kaminer, Enric Xargay, Vladimir Dobrokhodov,
Naira Hovakimyan, A. Pedro Aguiar, and António M. Pascoal

***Abstract*— This paper focuses on the problem of developing control laws to solve the *Time-Coordinated 3D Path-Following* task for multiple quadrotor UAVs in the presence of time-varying communication networks and spatial and temporal constraints. The objective is to enable a fleet of quadrotors to track predefined spatial paths while coordinating to achieve synchronization in both time and heading. One scenario is a symmetric exchange of position by four quadrotors initially positioned in four corners of a square room. When the mission starts, every quadrotor is required to execute collision free maneuvers and arrive at the opposite corner at the same desired instant of time. In this paper, the time-coordination task is solved by adjusting the second derivative of the coordination variable along the desired paths. Conditions are derived under which the coordination and path-following errors converge to a neighborhood of zero. Flight test results are presented to validate the theoretical findings.**

I. Introduction

Avoiding harm's ways requires the employment of intelligent autonomous vehicles. This, along with recent advances in miniature technology, brings a global spotlight on the development of Unmanned Aerial Vehicles (UAVs). Currently, the use of UAVs plays a crucial role in preventing exposure of human beings to uncertain and hostile environments, therefore avoiding any danger to the lives of operators. For instance, after being struck by the biggest recorded earthquake and a devastating tsunami, Japan has been fighting a potential nuclear catastrophe by deploying UAVs in situations where the presence of human operators was hazardous.

From a design point of view, and with a slight abuse of terminology, UAVs can be classified in two main categories: fixed-wings and rotatory-wings. Compared to the fixed-wings –which cannot freely move in any direction (rotate) or hold a constant position–, rotorcrafts can be deployed in a much wider variety of scenarios. Among rotatory-wings aircraft, quadrotors play an important role in research areas as prototypes for real-life missions, including monitoring and exploration of small areas.

A quadrotor consists of four blades, whose motion control is achieved by adjusting the angular rate of one or more rotor discs. Control of quadrotors is quite challenging and has been addressed in many recent publications. To mention a few, in [1] and [2] a stabilization and control algorithm is developed using Lyapunov stability theory. In [3] and [4] PD^2 and PID architectures are compared with LQR based control theory. Backstepping control is proposed in [5], while in [6] and [7] a visual-based feedback control law is presented using camera measurements for pose estimation. Fuzzy-logic control techniques are proposed in [8]. Intelligent control, based on neural networks, is introduced in [9] to achieve vertical take-off and landing. Integral sliding mode and reinforcement learning control are presented in [10] as solutions for accommodating the nonlinear disturbances for outdoor altitude control. Finally, in [11] a trajectory-tracking control algorithm is formulated using the Special Orthogonal group $\mathsf{SO}(3)$ for attitude representation, leading to a simple and singularity-free solution for the trajectory tracking problem.

Cooperation between multiple unmanned vehicles has also received significant attention in the control community in recent years. Relevant work includes spacecraft formation flying [12], UAV control [13], [14], coordinated control of land robots [15], and control of multiple autonomous underwater vehicles [16], [17]. However, much work remains to be done to overcome numerous critical constraints. For example, one of the crucial problems is the presence of time-varying communication networks that arise due to temporary loss of communication links and switching communication topologies [18], [19].

Motivated by these challenges, we address the problem of *Time-Coordinated 3D Path-Following* (TCPF), where a set of quadrotor UAVs are requested to *converge to and follow desired prespecified paths under stringent temporal constraints*. In the solution adopted, the path-following (PF) and time-coordination (TC) problems are almost decoupled. At the PF level, we assume there exists a control law capable of steering a quadrotor along its assigned path. At the TC level, the synchronization problem is solved by adjusting the commanded position and velocity of the quadrotors involved in the mission, thus obtaining –indirectly– vehicle coordination. Figure 1 captures the key concept described above.

This paper is organized as follows. In Section II, we define the PF and TC control problems, and present stability-related properties that the PF closed-loop system must satisfy. Then, a formal definition of the TCPF problem is given. In Section III we propose a solution for the TC problem. Section IV formulates a PF algorithm that enables an

Research is supported in part by USSOCOM, ONR, AFOSR, ARO, and CO3AUVs of the EU.

V. Cichella, E. Xargay, and N. Hovakimyan are with UIUC, Urbana, IL 61801, e-mail: {cichell2,xargay,nhovakim}@illinois.edu. I. Kaminer and V. Dobrokhodov are with NPS, Monterey, CA 93943, email: {kaminer,vldobr}@nps.edu. P. Aguiar and A. Pascoal are with IST, Lisbon, 1049 Portugal, email: pedro,antonio@isr.ist.utl.pt.

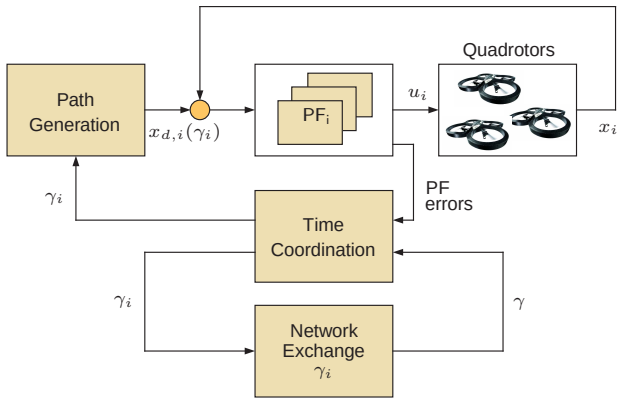

Fig. 1. TCPF Control Scheme.

AR.Drone quadrotor to follow a desired path, and shows that the convergence properties of the TCPF system hold for this particular vehicle. Section V presents and discusses flight tests results that illustrate the effectiveness of the proposed PF and TC algorithms. Finally, Section VI contains the main conclusions.

II. Problem Formulation

A. 3D Path-Following for a single quadrotor

Let $\mathcal{I}$ denote an inertial reference frame, and let $x_i(t) \in \mathbb{R}^3$ be the position of the center of mass of the ith quadrotor in this inertial frame, resolved in $\mathcal{I}$. Also, let $\mathcal{B}_i = \{\vec{b}_1, \vec{b}_2, \vec{b}_3\}$ denote the body frame with its origin located at the center of mass of the ith quadrotor; vector $\vec{b}_3$ is normal to the plane defined by the centers of the four rotors –pointing upwards in non-inverted flight–, while vectors $\vec{b}_1$ and $\vec{b}_2$ lie in this plane, with $\vec{b}_1$ pointing out the nose and $\vec{b}_2$ completing the right-hand system. Further, let $x_{d,i}(\gamma_i) \in \mathbb{R}^3$ be a desired path parameterized by γ_i, and assume that

$$\left\| \frac{\partial x_{d,i}}{\partial \gamma_i} \right\| \leq v_{d\max,i}\,, \tag{1}$$

for some $0 < v_{d\max,i} < v_{\max}$, where $v_{\max}$ is the maximum operational speed of the quadrotors. The choice of the parameterizing variable γ_i will be discussed later.

Then, we can define the position error vector as

$$e_{x,i} = x_{d,i}(\gamma_i) - x_i \ \in \mathbb{R}^3 \tag{2}$$

and the velocity error vector as

$$e_{v,i} = \frac{\partial x_{d,i}(\gamma_i)}{\partial \gamma_i}\,\dot{\gamma}_i - \dot{x}_i = \dot{x}_{d,i}(\gamma_i) - \dot{x} \ \in \mathbb{R}^3\,. \tag{3}$$

Additionally, similar to [11], define the errors

$$e_{\tilde{R},i} = \frac{1}{2}\left(R_{d,i}^\top R_i - R_i^\top R_{d,i}\right)^\vee\,, \tag{4}$$

$$e_{\Omega,i} = \Omega_i - R_i^\top R_{d,i}\Omega_{d,i}\,, \tag{5}$$

where $R_i \in \mathsf{SO(3)}$ and $\Omega_i \in \mathbb{R}^3$ are, respectively, the rotation matrix from the body-fixed frame $\mathcal{B}_i$ to the inertial frame $\mathcal{I}$ and the angular velocity of the ith quadrotor in the body-fixed frame $\mathcal{B}_i$; $R_{d,i} \in \mathsf{SO(3)}$ represents the desired attitude of the ith quadrotor with respect to the inertial frame and is generally expressed as a function of the position and velocity errors, $e_{x,i}$ and $e_{v,i}$, as well as the desired heading $\psi_{d,i}$; $\Omega_{d,i}$ satisfies $S(\Omega_d) = R_d^\top \dot{R}_d$; while the operators $(\cdot)^\vee$ and $S(\cdot)$ denote the *vee* and *hat* maps [11].

With the above notation, we define the path-following generalized error vector

$$x_{PF,i} = \left[e_{x,i}^\top,\ e_{v,i}^\top,\ e_{\tilde{R},i}^\top,\ e_{\Omega,i}^\top\right]^\top \ \in \mathbb{R}^{12}\,. \tag{6}$$

The dynamics of the ith vehicle's PF error vector can be modeled as

$$\dot{x}_{PF,i} = f_i(x_{PF,i}, u_i)\,, \tag{7}$$

where $f_i(\cdot)$ is a general nonlinear vector map and u_i is the control signal vector. Then, the PF control problem can be defined as:

Problem 1 (Path-Following Problem): Consider the ith quadrotor UAV and a given trajectory $x_{d,i}(\gamma_i)$ satisfying (1). We say that a controller $u_i(t)$ solves the PF control problem if the generalized PF error vector $x_{PF,i}$ with the dynamic described in (7) satisfies

$$\|x_{PF,i}(t)\| \leq k\|x_{PF,i}(0)\|e^{-\lambda_{PF}t}\,,$$

for some parameter $k > 0$, rate of convergence $\lambda_{PF} > 0$, and domain of attraction

$$D = \{x_{PF,i} \in \mathbb{R}^{12} \ :\ \|x_{PF,i}\| \leq r\}\,, \qquad r > 0\,.$$

Assumption 1: We assume that there exists a control law $u_i(t)$ that solves the PF problem defined in Problem 1.

B. Time-Coordination

We now address the TC problem of a fleet of n quadrotor UAVs. As will become clear, this problem will be solved by adjusting –for each vehicle– the second derivative of the parameterizing variable $\gamma_i(t)$.

As described earlier, the desired path assigned to each vehicle is parameterized by a variable γ_i, $i = 1, \ldots, n$. The choice of the parameter γ_i is such that, if $\gamma_i(t) - \gamma_j(t) = 0$, $\forall i, j \in \{1, \ldots, n\}$, $i \neq j$ and $\dot{\gamma}_i(t) = 1$, $\forall i \in \{1, \ldots, n\}$, at some time t, then all the vehicles are synchronized and evolve at the desired speed.

To achieve synchronization, the coordination variables γ_i have to be exchanged among the quadrotors over a supporting communications network. Using tools from graph theory, we can model the information flow as well as the constraints imposed by the communication topology. We start by assuming that the ith UAV communicates only with a neighboring set of vehicles, denoted by $\mathcal{N}_i$. We also assume that the communication between two UAVs is bidirectional with no delays. The reader is referred to [20] for key concepts and details on algebraic graph theory.

Following the notation used in [21], we now let $L(t) \in \mathbb{R}^{n\times n}$ be the Laplacian of the graph $\Gamma(t)$. Let $Q \in \mathbb{R}^{(n-1)\times n}$ be a matrix such that $Q1_n = 0$, $QQ^\top = I_{n-1}$, and define $\bar{L}(t) = QL(t)Q^\top$; it can be shown

that $\bar{L} \in \mathbb{R}^{(n-1)\times(n-1)}$ has the same spectrum as the Laplacian $L(t)$ without the eigenvalue $\lambda_1 = 0$. Finally, we let $\bar{L}(t)$ satisfy the persistency of excitation (PE) assumption:

$$\int_t^{t+T} \bar{L}(\tau)d\tau \geq \mu I_{n-1}\,. \tag{8}$$

Next, letting $\gamma(t) = [\gamma_1(t), \ldots, \gamma_n(t)]^\top$ and $\dot{\gamma}(t) = [\dot{\gamma}_1(t), \ldots, \dot{\gamma}_n(t)]^\top$, we define the coordination error vectors

$$\xi(t) = Q\gamma(t) \qquad \in \mathbb{R}^{n-1}\,, \tag{9}$$
$$z(t) = \dot{\gamma}(t) - 1_n \qquad \in \mathbb{R}^{n}\,. \tag{10}$$

From the definition of Q it follows that, if $\xi(t) = 0_n$, then $\gamma_i - \gamma_j = 0$, $\forall i, j \in \{1, \ldots, n\}$. Note that convergence of $z(t)$ to zero implies that the individual parameterizing variables $\gamma_i(t)$ evolve at the desired rate 1.

With the above notation, the coordination problem can now be defined as:

Problem 2 (Time-Coordination Problem): Given a set of n 3D desired trajectories $x_{d,i}(\gamma_i)$, design feedback control laws for $\ddot{\gamma}_i$ for all vehicles such that the coordination error vectors ξ and z, defined in (9) and (10) respectively, converge exponentially to a neighborhood of zero with rate of convergence $\lambda_{TC} > 0$.

C. Time-Coordinated 3D Path-Following

Considering the PF and TC problems described above, we can now define the combined TCPF control problem for a fleet of quadrotor UAVs.

Problem 3 (Time-Coordinated Path-Following Problem): Consider a set of n quadrotor UAVs and a set of n 3D desired trajectories $x_{d,i}(\gamma_i)$. Assume the quadrotors can communicate over a communications network satisfying (8). Design feedback control laws $u_i(t)$ and $\ddot{\gamma}_i(t)$ such that

1) for each vehicle, the generalized PF error vector $x_{PF,i}(t)$ defined in (6) converges to a neighborhood of zero;
2) the coordination error vectors defined in (9) and (10) converge exponentially to zero.

III. Time-Coordinated 3D Path-Following: Main Result

To solve the TCPF problem, we let the evolution of $\gamma_i(t)$ be given by

$$\ddot{\gamma}_i = -b(\dot{\gamma}_i - 1) - a\sum_{j\in\mathcal{N}_i}(\gamma_i - \gamma_j) - d\,\bar{\alpha}_i(x_{PF,i})\,,$$
$$\gamma_i(0) = 0\,, \quad \dot{\gamma}_i(0) = 1\,,$$

where a, b, d are positive coordination control gains, while $\bar{\alpha}_i(x_{PF,i})$ is defined as

$$\bar{\alpha}_i(x_{PF,i}) = \frac{\dot{x}_{d,i}^\top e_{x,i}}{\|\dot{x}_{d,i}\| + \delta} + \frac{\dot{x}_{d,i}^\top e_{v,i}}{\|\dot{x}_{d,i}\| + \delta}\,,$$

with δ being a positive design parameter. The dynamics of $\gamma(t)$ can be written in compact form as

$$\ddot{\gamma} = -bz - aL\gamma - d\bar{\alpha}(x_{PF})\,, \quad \gamma(0) = 0_n,\ \dot{\gamma}(0) = 1_n\,, \tag{11}$$

where

$$x_{PF} = [x_{PF,1}^\top, \ldots, x_{PF,n}^\top]^\top \qquad \in \mathbb{R}^{12n}\,,$$
$$\bar{\alpha}(x_{PF}) = [\bar{\alpha}_1(x_{PF,1}), \ldots, \bar{\alpha}_n(x_{PF,n})]^\top \qquad \in \mathbb{R}^{n}\,.$$

Then, the Lemma below states the main result of this paper:

Lemma 1: Consider a set of n quadrotor UAVs and a set of n 3D desired trajectories $x_{d,i}(\gamma_i)$. Given n PF algorithms satisfying Assumption 1 and the coordination control law described in (11), then there exist control gains a, b, d, and δ that solve the TCPF control problem 3. In particular, it can be shown that the vector $x_{TCPF} = [x_{PF}^\top, \xi^\top, z^\top]^\top$ converges exponentially fast to a neighborhood of zero with rate of convergence

$$\lambda = \min(\lambda_{PF}\,,\ \lambda_{TC})\,, \tag{12}$$

where

$$\lambda_{TC} < \frac{\mu}{2T(1+n^2T)^2}\,, \tag{13}$$

and with domain of attraction

$$D_c \triangleq \left\{x_{TCPF} \in \mathbb{R}^{14n-1} \ :\ \|x_{PF,i}\| \leq r\right\}\,. \tag{14}$$

Proof. An outline of the proof is given in the Appendix. □

Remark 1: The rate of convergence λ_{PF} depends on the properties of the adopted PF control law. If the PF control law has a rate of convergence greater than λ_{TC}, then the rate of convergence of the TCPF system is equal to the rate of convergence of the TC algorithm.

Remark 2: Note that the rate of convergence of the TC algorithm strictly depends on the quality of the communication network (parameters μ and T).

IV. Illustrative Example: TCPF with AR.Drones

To test the performance of the algorithm presented in the previous section, we adopted the flying robot architecture realized by Parrot AR.Drone company. To this end, we first developed a PF algorithm that satisfies the conditions described in Section II and that uses the control input provided by the AR.Drone autopilot, which accepts control commands for linear velocity along the inertial vertical channel $\dot{z}$, Euler angles θ and ϕ for the horizontal motion, and yaw rate $\dot{\psi}$. Next, we reformulate the PF problem presented in Section II for this particular platform, and derive a PF algorithm based on simple linear control.

A. PF Error Dynamics

For simplicity, we write separately the horizontal and vertical motions:

$$x = [(\Pi x)^\top,\ e_3^\top x]^\top\,,$$
$$v = [(\Pi v)^\top,\ e_3^\top v]^\top\,,$$

where $v = \dot{x}$, while Π and e_3 are defined as

$$\Pi = \begin{bmatrix} 1 & 0 & 0 \\ 0 & 1 & 0 \end{bmatrix}, \qquad e_3 = \begin{bmatrix} 0 \\ 0 \\ 1 \end{bmatrix}.$$

Therefore, the dynamics of the quadrotor can be written as follows:

$$\begin{aligned} \mathcal{H}: & \begin{cases} \Pi\dot{x} = \Pi v \\ \Pi\dot{v} = \Pi \frac{f}{m} R e_3 \end{cases} \\ \mathcal{V}: & \begin{cases} e_3^\top \dot{x} = e_3^\top v \\ e_3^\top \dot{v} = e_3^\top \frac{f}{m} R e_3 - g \end{cases} \end{aligned} \tag{15}$$

where R can be expressed in terms of the Euler angles as:

$$\begin{aligned} R &= R_\phi R_\theta R_\psi \\ &= \begin{bmatrix} c\theta c\psi & s\phi s\theta c\psi - c\phi s\psi & c\phi s\theta c\psi + s\phi s\psi \\ c\theta s\psi & s\phi s\theta s\psi + c\phi c\psi & c\phi s\theta s\psi - s\phi c\psi \\ -s\theta & s\phi c\theta & c\phi c\theta \end{bmatrix}. \end{aligned}$$

Since the AR.Drone autopilot is designed to operate using small angle commands in ϕ and θ, we can linearize the dynamics in (15) to obtain:

$$\begin{aligned} \mathcal{H}: & \begin{cases} \Pi\dot{x} = \Pi v \\ \Pi\dot{v} = \frac{f}{m} \begin{bmatrix} c\psi & -s\psi \\ s\psi & c\psi \end{bmatrix} \begin{bmatrix} \theta \\ -\phi \end{bmatrix} \end{cases} \\ \mathcal{V}: & \begin{cases} e_3^\top \dot{x} = e_3^\top v \\ e_3^\top \dot{v} = \frac{f}{m} - g \end{cases} \end{aligned} \tag{16}$$

Next, define the horizontal position and velocity errors as

$$e_{x_{xy}} = \Pi(x_d - x), \tag{17}$$
$$e_{v_{xy}} = \Pi(\dot{x}_d - \dot{x}). \tag{18}$$

Similarly, define the vertical position and velocity errors as

$$e_{x_z} = e_3^\top (x_d - x), \tag{19}$$
$$e_{v_z} = e_3^\top (\dot{x}_d - \dot{x}). \tag{20}$$

Also, let $e_{\tilde{R}}$ be defined as in (4) with $R_d = R_\phi R_\theta R_{\psi_d}$. This implies that

$$\begin{aligned} R_d^\top R &= R_{\psi_d}^\top R_\theta^\top R_\phi^\top R_\phi R_\theta R_\psi \\ &= R_{\psi_d}^\top R_\psi \\ &= \begin{bmatrix} c(\psi_d - \psi) & s(\psi_d - \psi) & 0 \\ -s(\psi_d - \psi) & c(\psi_d - \psi) & 0 \\ 0 & 0 & 1 \end{bmatrix}, \end{aligned}$$

thus leading to

$$e_{\tilde{R}} = \begin{bmatrix} 0 \\ 0 \\ -s(\psi_d - \psi) \end{bmatrix}.$$

Ignoring the first two components of $e_{\tilde{R}}$, we define

$$e_\psi = -s(\psi_d - \psi) \quad \in \mathbb{R}.$$

If we now consider small heading deviations with respect to the desired value ψ_d, then e_ψ can be approximated by

$$e_\psi = \psi - \psi_d. \tag{21}$$

Finally, define the generalized PF error vector as

$$x_{PF}^* = [e_{x_{xy}}^\top,\ e_{x_z},\ e_{v_{xy}}^\top,\ e_\psi]^\top \in \mathbb{R}^6 \tag{22}$$

Notice that, in contrast to the general formulation in Section II, the generalized error vector defined here does not consider the error states e_{v_z} and e_Ω. This is due to the fact that these two error signals are directly controlled by the AR.drone autopilot, ensuring their convergence to a neighborhood of zero.

With this in mind, we can now write the PF error dynamics as

$$\begin{cases} \dot{e}_{x_{xy}} &= e_{v_{xy}}, \\ \dot{e}_{v_{xy}} &= \Pi\ddot{x}_d - (e_3^\top \dot{v} + g) \begin{bmatrix} c\psi & -s\psi \\ s\psi & c\psi \end{bmatrix} u_1, \\ \dot{e}_{x_z} &= e_3^\top \dot{x}_d - u_2, \\ \dot{e}_\psi &= u_3 - \dot{\psi}_d, \end{cases} \tag{23}$$

where

$$u_1 = \begin{bmatrix} \theta \\ -\phi \end{bmatrix}, \quad u_2 = e_3^\top v, \quad u_3 = \dot{\psi}$$

are the command signals accepted by the AR.drone autopilot.

B. PF Control Law

Before we define the PF control law for the AR.drone quadrotor, we make the following assumption.

Assumption 2: The PID controller of the AR.drone autopilot responsible for $\dot{z}$ control is tuned to ensure that

$$e_3^\top \dot{v} + g > 0.$$

With this assumption, we can now define the control inputs u_1, u_2, and u_3 as

$$\begin{aligned} u_1 &= \frac{1}{(e_3^\top \dot{v} + g)} \begin{bmatrix} c\psi & s\psi \\ -s\psi & c\psi \end{bmatrix} (\Pi\ddot{x}_d + k_p e_{x_{xy}} + k_d e_{v_{xy}}), \\ u_2 &= e_3^\top \dot{x}_d + k_z e_{x_z}, \\ u_3 &= \dot{\psi}_d - k_\psi e_\psi, \end{aligned} \tag{24}$$

where k_p, k_d, k_z, and k_ψ are positive control gains. Then, it can be shown that the origin of the PF error dynamics (23) is (locally) exponentially stable. The next lemma summarizes this result.

Lemma 2: Consider an AR.drone quadrotor and a desired path $x_d(\gamma)$. Let the command signals of the AR.drone autopliot be given by (24) and assume $\|\dot{x}_d\| \leq v_{\max}$. Then, for any $\lambda_{PF}^* > 0$, there exist control gains k_p, k_d, k_z, and k_ψ such that the error vector defined in (22) satisfies

$$\|x_{PF}^*(t)\| \leq k\|x_{PF}^*(0)\| e^{-\lambda_{PF}^* t}$$

within some domain of attraction

$$D = \{x_{PF}^* \in \mathbb{R}^6 \ : \ \|x_{PF}^*\| \leq r^*\}, \tag{25}$$

where the linearization of the quadrotor dynamics is valid.

Proof. The proof of this result is omitted due to space limitations. □

Corollary 1: Consider a set of n AR.Drone quadrotors and a set of n 3D desired trajectories $x_{d,i}(\gamma_i)$. Given n PF algorithms proposed in Lemma 2 and the coordination control law described in (11), there exist control gains a, b,

d, and δ that solve the TCPF control problem 3 with rate of convergence

$$\lambda = \min(\lambda^*_{PF}\,,\ \lambda_{TC})\,,$$

where λ^*_{PF} is defined in Lemma 2 and

$$\lambda_{TC} < \frac{\mu}{2T(1+n^2T)^2}\,,$$

and with domain of attraction

$$D^*_c = \left\{x_{TCPF} \in \mathbb{R}^{8n-1} \quad : \quad \|x_{PF,i}\| \leq r^*\right\}. \qquad (26)$$

Remark 3: The bound r^* in (25) for which the linearization of the quadrotor dynamics is valid will depend on the choice of the control gains k_p, k_d, k_z, and k_ψ. A relation between these control gains and r^* can be obtained from the control laws in (24).

V. Flight Test Results

In this section, we present flight tests results of two AR.Drone quadrotors that are tasked to follow circular, planar paths of radius 2 m at a constant speed, while synchronizing both their phase-on-orbit and their headings.

To solve this problem, we use the PF algorithm described in the previous section and the coordination control law proposed in Section III. Figure 2 presents the results of this experiment. In particular, Figure 2a shows the desired orbit (black) and the actual trajectories of the two quadrotors (blue and red). Since the two UAVs are tasked to follow the same orbit, a phase-on-orbit separation is required between the two vehicles to avoid collision. This separation is specified online from the ground station, and it varies according to mission requirements. The desired phase-on-orbit separation, along with the actual phase separation between the two UAVs, is shown in Figure 2b. In this particular scenario, the UAVS are initially required to keep a 180-deg phase separation; at approximately $t = 94$ s, the required phase separation goes down to 90 deg; the two quadrotors keep this configuration for about 14 s, when the required phase separation goes back to 180 deg; finally, in the last part of the experiment, the UAVs are required to keep a phase separation of 270 deg.

The performance of the PF algorithm is illustrated in Figure 2c for both quadrotors. As can be seen in the figure, the PF algorithm is able to steer the quadrotors along the circular paths. Note that the deviations appearing at times 94, 112, and 123 s are due to the sudden changes in desired phase separation. Finally, Figure 2d shows the convergence of $\dot\gamma_1$ and $\dot\gamma_2$ to the desired rate 1, as well as the convergence of the coordination errors to a neighborhood of zero.

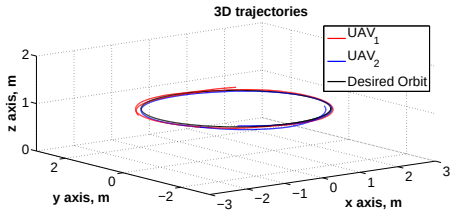

(a) Desired and actual orbits.

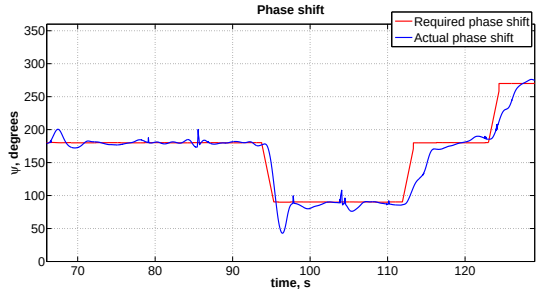

(b) Desired and actual phase separation.

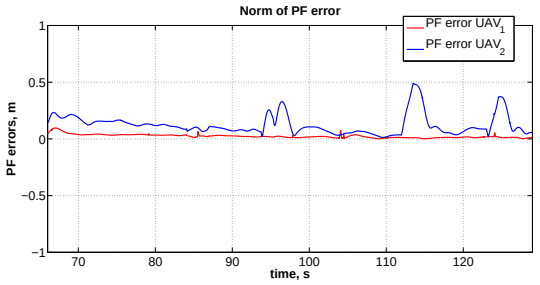

(c) PF error.

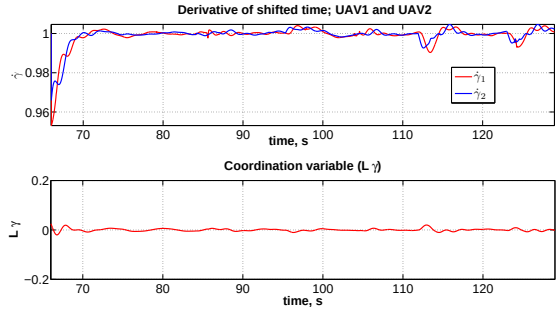

(d) Coordination errors.

Fig. 2. Flight test results with two AR.Drone UAVs.

VI. Conclusion

This paper addressed the problem of steering a fleet of quadrotor UAVs along predefined spatial paths, while coordinating with each other according to mission requirements. Cooperative control is achieved in the presence of time-varying communication networks, and stringent temporal constraints. The constraints include collision-free maneuvers (generated off line) and simultaneous arrival at the desired locations. The proposed solution solves the time-coordination problem under the assumption that a path-following algorithm –meeting certain stability conditions– is given. The synchronization task is accomplished by adjusting the desired position and velocity of each vehicle. The exponential convergence of the time-coordination error is proven using Lyapunov theory. An illustrative example is presented to validate the convergence of the algorithm. To this end, an ad-hoc path-following algorithm is formulated and implemented for two AR.Drone quadrotors. The results obtained validate the theoretical findings.

REFERENCES

[1] S. Bouabdallah, P. P. Murrieri, and R. Siegwart, "Design and control of an indoor micro quadrotor," in *Proc. of The International Conference on Robotics and Automation (ICRA)*, 2004.

[2] A. Dzul, P. Castillo, and R. Lozano, "Real-time stabilization and tracking of a four rotor mini rotorcraft," in *IEEE Transaction on Control System Technology*, vol. 12(4), 2004, pp. 510–516.

[3] A. Tayebi and S. McGilvray, "Attitude stabilization of a vtol quadrotor aircraft," in *IEEE Transaction on Control System Technology*, vol. 14(3), May 2006, pp. 562–571.

[4] S. Bouabdallah, A. Noth, and R. Siegwart, "Pid vs lqr control techniques applied to an indoor micro quadrotor," in *International Conference on Intelligent Robots and Systems*, 2004.

[5] N. Guenard, T. Hamel, and V. Moreau, "Dynamic modeling and intuitive control strategy for an x4-flyer," in *International Conference on Robotics and Automation (ICRA)*, 2005, pp. 141–146.

[6] E. Altug, J. P. Ostrowski, and R. Mahony, "Control of a quadrotor helicopter using visual feedback," in *Proc. of the 2002 IEEE International Conference on Robotics and Automation (ICRA)*, 2002, pp. 72–77.

[7] N. Guenard, T. Hamel, and R. Mahony, "A practical visual servo control for an unmanned aerial vehicle," in *IEEE Transaction on Robotics*, vol. 24(2), 2008, pp. 331–340.

[8] C. Coza and C. J. B. Macnab, "A new robust adaptive-fuzzy control method applied to quadrotor helicopter stabilization," in *Annual meeting of the North American Fuzzy Information Processing Society*, 2006, pp. 454–458.

[9] M. Tarbouchi, J. Dunfied, and G. Labonte, "Neural network based control of a four rotor helicopter," in *International Conference on Industrial Technology*, 2004, pp. 1543–1548.

[10] S. L. Waslander, G. M. Hoffman, J. S. Jang, and C. J. Tomlin, "Multi-agent quadrotor testbed control design: integral sliding mode vs reinforcement learning," in *International Conference on Intelligent Robots and Systems*, 2005, pp. 468–473.

[11] T. Lee, M. Leok, and N. H. McClamroch, "Control of complex maneuvers for a quadrotor UAV using geometric methods on SE(3)," *IEEE Transactions on Automatic Control*, 2010, submitted. Available online: `arXiv:1003.2005v3`.

[12] M. Mesbahi and F. Y. Hadaegh, "Formation flying control of multiple spacecraft via graphs, matrix inequalities, and switching," *Journal of Guidance, Control and Dynamics*, vol. 24, no. 2, pp. 369–377, March–April 2001.

[13] Y. D. Song, Y. Li, and X. H. Liao, "Orthogonal transformation based robust adaptive close formation control of multi-UAVs," in *American Control Conference*, vol. 5, Portland, OR, June 2005, pp. 2983–2988.

[14] D. M. Stipanović, G. İnalhan, R. Teo, and C. J. Tomlin, "Decentralized overlapping control of a formation of unmanned aerial vehicles," *Automatica*, vol. 40, no. 8, pp. 1285–1296, August 2004.

[15] R. Ghabcheloo, A. M. Pascoal, C. Silvestre, and I. Kaminer, "Coordinated path following control of multiple wheeled robots using linearization techniques," *International Journal of Systems Science*, vol. 37, no. 6, pp. 399–414, May 2006.

[16] R. Ghabcheloo, A. P. Aguiar, A. M. Pascoal, C. Silvestre, I. Kaminer, and J. P. Hespanha, "Coordinated path-following control of multiple underactuated autonomous vehicles in presence of communication failures," in *IEEE Conference on Decision and Control*, San Diego, CA, December 2006, pp. 4345–4350.

[17] F. L. Pereira and J. B. de Sousa, "Coordinated control of networked vehicles: An autonomous underwater system," *Automation and Remote Control*, vol. 65, no. 7, pp. 1037–1045, July 2004.

[18] I. Kaminer, A. M. Pascoal, E. Hallberg, and C. Silvestreo, "Trajectory tracking for autonomous vehicles: An integrated approach to guidance and control," *Journal of Guidance, Control and Dynamics*, vol. 21, no. 1, pp. 29–38, January–February 1998.

[19] Y. Kim and M. Mesbahi, "On maximizing the second smallest eigenvalue of state-dependent graph Laplacian," *IEEE Transactions on Automatic Control*, vol. 51, no. 1, pp. 116–120, January 2006.

[20] N. Biggs, *Algebraic Graph Theory*. New York, NY: Cambridge University Press, 1993.

[21] E. Xargay, I. Kaminer, A. Pascoal, N. Hovakimyan, V. Dobrokhodov, V. Cichella, A. P. Aguiar, and R. Ghabcheloo, "Time-critical cooperative path following of multiple uavs over time-varying networks," 2012, accepted for publication in *AIAA Journal of Guidance, Control and Dynamics*.

[22] H. K. Khalil, *Nonlinear Systems*. Englewood Cliffs, NJ: Prentice Hall, 2002.

[23] A. Loría and E. Panteley, "Uniform exponential stability of linear time-varying systems: Revisited," *Systems & Control Letters*, vol. 47, no. 1, pp. 13–24, September 2002.

APPENDIX
SKETCH OF THE PROOF OF LEMMA 1

Assuming that the PF system (7) satisfies Assumption 1, and following the same argument as in [22, Theorem 4.14], there exists a Lyapunov function satisfying

$$c_1||x_{PF}||^2 \leq V_{PF} \leq c_2||x_{PF}||^2\,, \quad \dot{V}_{PF} \leq -c_3||x_{PF}||^2\,. \tag{27}$$

In addition, consider the system

$$\dot{\phi}(t) = -\bar{L}\phi(t)\,. \tag{28}$$

Since the matrix $\bar{L}$ satisfies the PE condition in (8), we can use the result in [23, Lemma 5] to conclude that the system in (28) is GUES (global uniformly exponentially stable), and that the following bound holds:

$$||\phi(t)|| \leq k_\lambda||\phi(0)||e^{-\gamma_\lambda t}$$

with $k_\lambda = 1$ and $\gamma_\lambda \geq \bar{\gamma}_\lambda = \frac{\mu}{T(1+n^2T)^2}$. This, together with [23, Lemma 1] or a similar argument as the one in [22, Theorem 4.14], imply that there exists a continuosly differentiable, symmetric, positive definite matrix $P_c(t)$ that satisfies the following inequalities:

$$\begin{aligned} &0 < \bar{c}_1 I \triangleq \frac{\bar{c}_3}{2n} I \leq P_c(t) \leq \frac{\bar{c}_4}{2\gamma_\lambda} I \triangleq \bar{c}_2 I \\ &\dot{P}_c - \bar{L}P_c - P_c\bar{L} \leq -\bar{c}_3 I\,. \end{aligned} \tag{29}$$

Next, introducing the transformation

$$\chi(t) = b\xi + Qz\,,$$

the time coordination states can be redefined as $x_{TC} = [\chi^\top, z^\top]^\top$, with dynamics

$$\begin{cases} \dot{\chi} = -\frac{a}{b}\bar{L}\chi + \frac{a}{b}QLz - Q\bar{\alpha}(x_{PF}) \\ \dot{z} = -(bI - \frac{a}{b}L)z - \frac{a}{b}LQ^\top\chi - \bar{\alpha}(x_{PF})\,. \end{cases} \tag{30}$$

At this point, we choose a Lyapunov candidate function

$$V = V_{PF} + \frac{1}{2}\chi^\top P_c\chi + \frac{\beta_1}{2}||z||^2\,, \tag{31}$$

where $\beta_1 > 0$, and V_{PF} and P_c were introduced above. After some mathematical computations, and using (27), (29), and (30), the derivative of the Lyapunov function becomes:

$$\begin{aligned} \dot{V} \leq &-\left(c_3 - (\beta_1 + \bar{c}_2)d\frac{v_{d\max}}{v_{d\max} + \delta}\right)||x_{PF}||^2 \\ &-\left(\frac{\bar{c}_3}{2} - 2\bar{c}_2 d\frac{v_{d\max}}{v_{d\max} + \delta}\right)||\chi||^2 \\ &-\beta_1\left(b - n - 2d\frac{v_{d\max}}{v_{d\max} + \delta}\right)||z||^2 \\ &+\chi^\top(P_cQL - \beta_1 QL)z\,. \end{aligned}$$

At this point, one can show that there exist b, d, δ, $\bar{c}_2$, and $\bar{c}_3$ such that

$$\begin{aligned} \dot{V} &\leq -2\lambda V\,, \\ \|\dot{\gamma}\|_\infty &\leq \frac{v_{\max}}{v_{d\max}}\,, \end{aligned}$$

where λ was defined in (12). The second bound above is required to show feasibility of the commanded speed profile. This completes the proof. □